Diketopyrrolopyrrole-Based Liquid Crystalline Conjugated Donor–Acceptor Copolymers with Reduced Band Gap for Polymer Solar Cells

Yunli Han,[1] **Lie Chen,**[1,2] **Yiwang Chen**[1,2]

[1]Institute of Polymers/Department of Chemistry, Nanchang University, 999 Xuefu Avenue, Nanchang 330031, China
[2]Jiangxi Provincial Key Laboratory of New Energy Chemistry, Nanchang University, 999 Xuefu Avenue, Nanchang 330031, China
Correspondence to: Y. Chen (E-mail: ywchen@ncu.edu.cn) or L. Chen (E-mail: chenlienc@163.com)

Received 21 July 2012; accepted 25 September 2012; published online 23 October 2012
DOI: 10.1002/pola.26394

ABSTRACT: A new liquid crystalline (LC) acceptor monomer 2,5-bis[4-(4′-cyanobiphenyloxy)dodecyl]-3,6-dithiophen-2-yl-pyrrolo[3,4-c]pyrrole-1,4-dione (TDPPcbp) was synthesized by incorporating cyanobiphenyl mesogens into diketopyrrolopyrrole (DPP). The monomer was copolymerized with bis(2-ethylhexyloxy)-benzo[1,2-b:4,5-b′] dithiophene (BDT) and *N*-9′-heptadecanylcarbazole (CB) donors to obtain donor–acceptor alternating copolymers poly[4,8-bis(2-ethylhexyloxy)benzo[1,2-b:4,5-b′] dithiophene-alt-3,6-bis(thiophen-5-yl)-2,5-bis[4-(4′-cyanobiphenyloxy)dodecyl]-2,5-dihydropyrrolo[3,4-c]pyrrole-1,4-dione] (PBDTDPPcbp) and poly[N-9′-heptadecanyl-2,7-carbazole-alt-3,6-bis(thiophen-5-yl)-2,5-bis[4-(4′-cyano-biphenyloxy)dodecyl]-2,5-dihydropyrrolo[3,4-c]pyrrole-1,4-dione] (PCBTDPPcpb) with reduced band gap, respectively. The LC properties of the copolymers, the effects of main chain variation on molecular packing, optical properties, and energy levels were analyzed. Incorporating the mesogen cyanobiphenyl units not only help polymer donors to pack well through mesogen self-organization but also push the fullerene acceptor to form optimized phase separation. The bulk heterojunction photovoltaicdevicesshow enhanced performance of 1.3% for PBDTDPPcbp and 1.2% for PCBTDPPcbp after thermal annealing. The results indicate that mesogen-controlled self-organization is an efficient approach to develop well-defined morphology and to improve the device performance. © 2012 Wiley Periodicals, Inc. J Polym Sci Part A: Polym Chem 51: 258–266, 2013

KEYWORDS: conjugated polymers; liquid crystals; liquid-crystalline polymers (LCP); morphology photovoltaics

INTRODUCTION In recent years, bulk heterojunction (BHJ) polymer solar cells (PSC) have attracted considerable interests as promising candidates for a new renewable energy source because of their low cost, potential for achieving large area, flexible photovoltaic devices with fast roll-to-roll production. PSCs are predicted to yield power conversion efficiency (PCE) up to a commercial level, if a suitable low band gap donor material is discovered. The research community has made great progress in the field of BHJ PSC. The PCE, a key parameter to assess the performance of PSC is over 8%.[1–6] However, the efficiency of PSC is still low compared with inorganic counterparts, which hinder their applications.

To obtain high-performance photovoltaic polymer materials, it is necessary to design and synthesize a new conjugated polymer with ideal properties, such as low band gap, broad absorption range, high hole mobility, and suitable molecular energy levels. One potential strategy is to make appropriate low-band gap polymers with tunable energy levels via the donor–acceptor (D–A) approach. The intramolecular charge transfer (ICT) between the electron-rich "donor" and the electron-deficient "acceptor" moieties can individually tune the band gap and energy levels of the conjugated polymer.[7] Due to the improvement of the PCE of the photovoltaic devices, D–A copolymers have been developed rapidly over past few years. Among various D–A copolymers, the polymers based on benzodithiophene (BDT)[8,9] and 2,7-carbazole (CB)[10] "push" units have been regarded as the most promising semiconductors for highly efficient BHJ solar cells.

Recently, a group of D–A copolymer based on diketopyrrolopyrrole (DPP)-based polymers that works well in field-effect transistors and solar cells are being discovered,[11–18] due to their desirable properties, such as low band gap, broad optical absorption, and high charge carrier mobility because of their strong π–π interaction and good planarity. Organic photovoltaic functional materials containing DPP core as donor have demonstrated great potential and achieved attractive efficiencies,[19] with the best hole mobility up to about 2 cm^2/V/s and extraordinary PCE over 5.5%.[12–15] However, a systematic study of DPP-based polymer donors to establish structure–property relationships, namely the nature of electronic structure and charge transport properties of polymer chain–chain

Additional Supporting Information may be found in the online version of this article.

interaction and alignment in solid state of organic photovoltaic (OPV) applications, has not been investigated.

To achieve the ordering and packing of organic donor materials and to overcome defect formation at the D–A interface, high-mobility liquid crystalline (LC) polymer with crystalline morphologies are introduced to control the phase separation between the two components in BHJ. Liquid crystals possess both order and mobility at molecular, supramolecular, and macroscopic levels, as a result of self-assembled dynamic functional soft materials.[20–27] In our previous studies, we have synthesized a new type D–A liquid-crystalline copolymer, PFcbpDTBT, via copolymerization of LC electron-donor fluorene and electron-acceptor dithienylbenzothiadiazole (DTBT) units, revealing that spontaneous self-organization of PFcbpDTBT can push [6,6]-phenyl-C61 butyric acid methyl ester (PCBM) clusters to an oriented nanodispersing structure.[28] This situation inspired us to design another type of LC D–A alternating copolymer, containing electron-accepting building block bearing LC side chain. Taking all of these results into account, here we report the synthesis of a new DPP monomer containing cyanobiphenyl mesogens and its application of copolymerization with bis(2-ethylhexyloxy) benzo[1,2-b:4,5-b′]dithiophene (BDT) or *N*-9′-heptadecanyl-2,7-carbazole (CB) to obtain polymers poly[4,8-bis(2-ethylhexyloxy)benzo[1,2-b:4,5-b′]dithiophene-alt-3,6-bis(thiophen-5-yl)-2,5-bis[4-(4′-cyanobiphenyloxy)dodecyl]-2,5-dihydropyrrolo[3,4-c]pyrrole-1,4-dione] (PBDTDPPcbp) and PCBTDPPcbp. We hope our work can shed light on the design of new organic electronic materials with optimized liquid-crystal side chain architecture.

EXPERIMENTAL

Measurements and Characterization

The ultraviolet (UV)–visible spectra of the copolymers were characterized on a PerkinElmer Lambda 750 spectrophotometer. Thermogravimetric analysis (TGA) measurements were carried out with PerkinElmer TGA 7 for thermogravimetry at a heating rate of 10°C/min under nitrogen. Differential scanning calorimetry (DSC) was used to study phase-transition temperatures on a Perkin-Elmer DSC 7 differential scanning calorimeter with a constant heating/cooling rate of 10 °C/min under a nitrogen flow. Texture observations were with studied by polarizing optical microscopy (POM) a Nikon E600POL polarizing optical microscope equipped with an Instec HS 400 heating and cooling stage. The X-ray diffraction (XRD) study of the copolymers was performed on a Bruker D8 Focus X-ray diffractometer operating at 30 kV and 20 mA with a copper target ($\lambda = 1.54$ Å) and at a scanning rate of 1 °/min. The gel permeation chromatography, so-called size-exclusion chromatography analysis, was conducted with a Knauer Smartline system equipped with a Rheodyne injector, using polystyrenes as the standard and $CHCl_3$ as the eluent at a flow rate of 1.0 mL/min and 40°C through a Styragel column set, Styragel HT3 and HT4 (19 mm × 300 mm, $10^3 + 10^4$ Å) to separate molecular weight ranging from 10^2 to 10^6. Cyclic voltammograms (CV) were carried out in a three-electrode cell using platinum electrodes at a scan rate of 50 mV/s and a Ag/Ag$^+$ (0.1 M of $AgNO_3$ in acetonitrile) reference electrode in an anhydrous and argon-saturated solution of 0.1 M of tetrabutylammonium tetrafluoborate (Bu_4NBF_4) in acetonitrile. Under these conditions, the oxidation potential ($E_{OX1/2}$) of ferrocene was -0.02 eV versus Ag/Ag$^+$. The HOMO energy level of polymers was determined from the oxidation onset of the second scan from CV data. It is assumed that the redox potential of Fc/Fc$^+$ has an absolute energy level of -4.40 eV to vacuum. The energy of HOMO and LUMO levels were calculated according to (1) and (2), and the electrochemically determined band gaps were deduced from the difference between onset potentials from oxidation and reduction of copolymers as depicted in (3).[30]

$$E_{\mathrm{HOMO}} = -(E^{\mathrm{ox}}_{\mathrm{red}} + 4.40)(\mathrm{eV}) \tag{1}$$

$$E_{\mathrm{LUMO}} = -(E^{\mathrm{red}}_{\mathrm{onset}} + 4.40)(\mathrm{eV}) \tag{2}$$

$$E_{\mathrm{g}} = (E^{\mathrm{ox}}_{\mathrm{red}} - E^{\mathrm{red}}_{\mathrm{onset}})(\mathrm{eV}) \tag{3}$$

Annealing of films was conducted by heating in the setting temperature for 10 min, followed by cooling to room temperature at a cooling speed of 1 °/min.

Device Fabrication and Characterization

The polymer PVCs were fabricated with the sandwiched structure of glass/indium-tin oxide (ITO)/[poly(3,4-ethylene dioxythiophene):poly(styrene sulfonate)] (PEDOT:PSS)/Polymer:PCBM (1:2)/Aluminum. Prior to use, the substrates were ultrasonicated for 30 min in acetone followed by detergent and deionized water and then 2-propanol. The substrates were dried under a nitrogen flow and subjected to the treatment of UV ozone over 20 min. A filtered dispersion of PEDOT:PSS in water (Baytron Al4083) was then spun-cast onto clean ITO substrates at 4000 rpm for 60 s and then baked at 120 °C. The copolymers were dissolved in dichlorobenzene to make 15 mg/mL for PBDTDPPcbp and 20 mg/mL for PCBTDPPcbp solutions, followed by blending with PCBM (purchased from Lumtec. Corp). The active layers were got by spin-coating the blend solutions at 800 rpm for 30 s. Subsequently, a 0.6 nm layer of LiF followed by a 100 nm layer of Al were evaporated under vacuum ($<10^{-6}$ Torr) to form the electrodes. The thicknesses of all the films were measured by a Dektak profiler. Annealing of some devices was conducted by heating at different temperatures for 10 min, followed by cooling to room temperature at a cooling speed of 1 °/min. Current–voltage (*J*–*V*) characteristics were recorded using Keithley 2400 Source Meter in the dark and under 100 mW/cm^2 simulated AM 1.5 G irradiation (Abet Solar Simulator Sun 2000). All the measurements were performed under ambient atmosphere at room temperature.

Materials

3,6-Dithiophen-2-yl-2,5-dihydro-pyrrolo[3,4-c]pyrrole-1,4-dione (TDPP), 4-cyanobiphenyloxy,2,7-bis(4,4,5,5-tetramethyl-1,3,2-dioxaboralan-2-yl)-*N*-9′-hepta-decanylcarbazole,2,6-bis(trimethyltin)-4,8-bis(2-ethylhexyloxy)-benzo[1,2-b:4,5-b′] dithiophene, 1,12-dibromododecane, tetrakis(triphenylphosphine) palladium, $PC_{60}BM$, and other materials are purchased from

Alfa Aesar, or Aldrich and used without further purification. ITO glass was purchased from Delta Technologies Limited, whereas PEDOT:PSS (Baytron PAl4083) was obtained from Bayer Inc. The following compounds were synthesized according to the procedure in the literature: PCBTDPPcbp[29] and PBDTDPPcbp[30]

4-(4′-Cyanobiphenyloxy)dodecylbromide (1)

In a 500-ml round bottom flask, a mixture of 4-cyanobiphenyloxy (3.9 g, 20 mmol), anhydrous potassium carbonate (19.6 g, 60 mmol), 1,12-dibromododecane (16.5 g, 120 mmol) was added and stirred in 300 ml acetone at 135 °C. The reaction mixture was refluxed with stirring for 24 h. After cooling down to the room temperature, the mixture was filtered and washed with acetone of 300 ml. The solvent was removed by reduced pressure, and the residue was dried by vacuum to get the crude product. Purification was accomplished by column chromatography on silica with hexane:dichloromethane = 1:2 to afford the product.

(Yield: 80%) ^{1}H NMR (CDCl$_3$, 400 Hz): δ (ppm) 7.70 (d, 2H), 7.65 (d, 2H), 7.53 (d, 2H), 7.00 (d, 2H), 4.01 (t, 2H), 3.19 (t, 2H), 1.9–0.8 (m, 20H).

2,5-Bis[4-(4′-Cyanobiphenyloxy)dodecyl]-3,6-dithiophen-2-yl-pyrrolo[3,4-c]pyrrole-1,4-dione (2)

In a 250-ml round bottom flask, 3,6-dithiophen-2-yl-2,5-dihydro-pyrrolo[3,4-c]-pyrrole-1,4-dione (DPP) (1.5 g, 5 mmol) and anhydrous K$_2$CO$_3$ (2.07 g, 15 mmol) were added under argon. The mixture was degassed three times, and then 150 ml anhydrous *N*,*N*-dimethylformamide was injected into the mixture and heated to 130 °C under argon for 3 h, compound **1** (8.85 g, 20 mmol) was added into the reaction solution. The reaction mixture was stirred for 24 h at 135 °C. The reaction mixture was allowed to cool down to the room temperature, poured into 300 ml of water, and stirred for 0.5 h. The water layer was extracted by 300 ml of CHCl$_3$ three times. The combined organic fractions were dried over magnesium sulfate, and the solvent was removed under reduced pressure. The solid was washed with several portions of distilled water and methanol alternatively. The crude product was purified by column chromatography using dichloromethane as eluent, and the solvent was evaporated under reduced pressure. A red powder is obtained.

(Yield: 70%) ^{1}H NMR (CDCl$_3$, 400 Hz): δ (ppm) 8.94 (d, 2H), 7.70 (d, 10H) 7.52 (d, 4H), 7.30 (d, 2H), 6.99 (d, 4H), 4.07 (t, 4H), 4.00 (t, 4H), 1.7–0.8 (m, 40H).

3,6-Bis-(5-Bromo-thiophen-2-yl)-2,5-bis[4-(4′-cyanobiphenyloxy)dodecyl]-pyrrolo-[3,4-c] pyrrole-1,4-dione (TDPPcbpBr) (3)

In a 250-ml round bottom flask, covered with aluminum foil, compound **2** (1.022 g, 1mmol) and *N*-bromosuccinimide (0.396 g, 2.2 mmol) were added, and then were dissolved into 80 ml of CHCl$_3$, at last, the reaction mixture was stirred for 48 h at room temperature. After that, the reaction mixture was poured into 300 ml of water, stirred for 0.5 h at room temperature, the solution was extracted by CHCl$_3$ three times, and the combined organic phase was washed by distilled water. The extraction solution was rotorary-evaprated under reduced pressure. The solid was then collected by vacuum filtration and washed with hot water and hot methanol alternatively. Then the crude product was purified by column chromatography using gradient elution (chloroform:hexanes = 10:3). A purple solid was obtained.

(Yield: 60%) ^{1}H NMR (CDCl$_3$, 400 Hz): δ (ppm) 8.66 (d, 2H), 7.69 (d, 4H), 7.64 (d, 4H), 7.53 (d, 4H), 7.24 (d, 2H), 6.96 (t, 4H), 4.01 (d, 4H), 3.97 (d, 4H), 2–0.9 (m, 40H)

Poly[N-9′-Heptadecanyl-2,7-carbazole-alt-3,6-bis(thiophen-5-yl)-2,5-bis[4-(4′-cyano-biphenyloxy) dodecyl]-2,5-dihydropyrrolo[3,4-c]pyrrole-1,4-dione] (PCBTDPPcbp)

Compound **3** (0.17745 g, 0.15 mmol), 2,7-bis(4,4,5,5-tetramethyl-1,3,2-dioxaboralan -2-yl)-*N*-9′-heptadecanylcarbazole (98.625 mg, 0.15 mmol), 3.5 mg (0.003 mmol) of K$_2$CO$_3$ (345 mg, 2.6 mmol) and tetrakis(triphenylphosphine)palladium(0) were dissolved in 8 ml of THF and 2.5 ml of H$_2$O. The reaction mixture was vigorously stirred at 85 °C, After 72 h, bromobenzene (2 μL, 0.015 mmol) was added into the reaction mixture, 3 h later, phenylboronic acid (2.15 mg, 0.015 mmol) was added, and the reaction mixture was refluxed overnight to complete the end capping reaction. The polymer was purified by precipitation by methanol/water (10:1), then filtered and washed on Soxhlet appartus with methanol, acetone, hexane, and chloroform. The chloroform fraction was condensed under reduced pressure, precipitated in methanol/H$_2$O (10:1, 250 ml), then filtered, and polymer was obtained after vacuum-drying at 50 °C overnight.

(yield: 65 %) ^{1}H NMR (CDCl$_3$, 400 Hz): δ (ppm) 9.13 (d, 2H), 8.21 (d, 2H), 7.87–7.4 (m, 18H), 7.0–6.93 (m, 7H), 4.62 (m, 1H), 4.21 (m, 4H), 3.94 (d, 4H), 2.36 (d, 4H), 2.0–1.0 (m, 78H), 0.8 (m, 4H).

PBDTDPPcbp

To a 100 ml flask, 2,6-bis(trimethyltin)-4,8-bis(2-ethylhexyloxy)-benzo[1,2-b:4,5-b′]dithiophene (BDT) (0.1158 g, 0.15 mmol), Compound **3** (0.17745 g, 0.15 mmol), and toluene (8 ml) were added. The system was purged with Ar under vacuum. Then (PPh$_3$)$_4$Pd(0) (0.03 g, 0.03 mmol) was added. The solution was stirred at 110 °C, and refluxed for 24 h under the protection of Ar. After the solution was cooled down to room temperature, the solution was dropped into acetone to precipitate the copolymer. The copolymer was Soxhlet extracted with methanol, acetone, hexane, and chloroform to remove oligmer, and then with chloroform to collect the polymer.

(Yield: 65.4%) ^{1}H NMR (CDCl$_3$, 400 Hz): 9.02 (d, 2H), 7.8–7.35 (m, 13H), 7.06 (m, 3H), 6.93 (d, 4H), 4.06 (d, 6H), 3.78 (d, 4H), 2.5–0.8 (m, 74H).

RESULTS AND DISCUSSION

Synthesis and Characterization

The synthesis of the copolymers PBDTDPPcbp and PCBTDPPcbp is outlined in Scheme 1. Alternating copolymer PBDTDPPcbp is synthesized via a Stille polycondensation

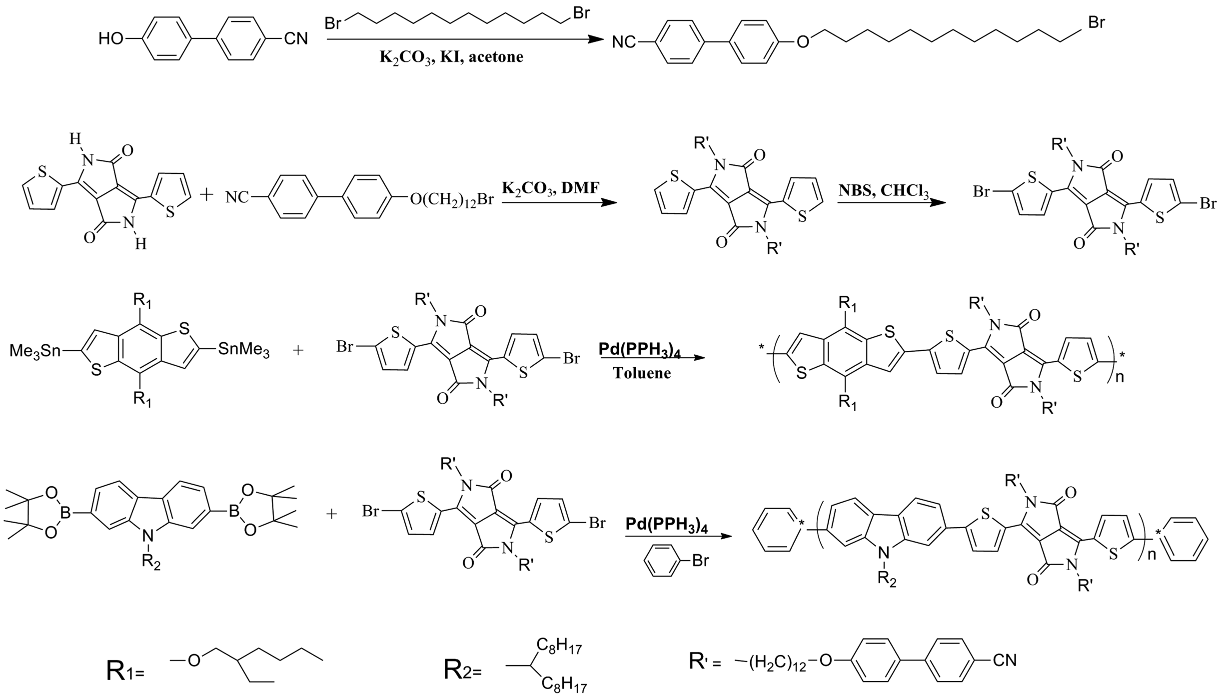

SCHEME 1 Synthesis of the LC monomer and D–A copolymer.

reaction, where 2,5-bis[4-(4′-cyanobiphenyloxy)dodecyl]-3,6-dithiophen-2-yl-pyrrolo[3,4-c]pyrrole-1,4-dione (TDPPcbp) was used as an electron acceptor unit and 2,6-bis(trimethyltin)-4,8-bis(2-ethylhexyloxy)benzo[1,2-b:4,5-b′]-dithiophene (BDT) was the donor unit. However, the copolymer of PCBTDPPcbp was synthesized by a Suzuki polycondensation reaction between 2,7-(bis(4,4,5,5- tetramethyl-1,3,2-dioxaboralan-2-yl)-*N*-9′-heptadecanylcarbazole (CB) and TDPPcbp. Both the copolymers were purified by Soxhlet extraction with methanol, acetone, hexane, and chloroform in succession. The identity and purity of the new monomer and copolymers have been confirmed by ^{1}H NMR (Supporting Information Figs. S1–S3).

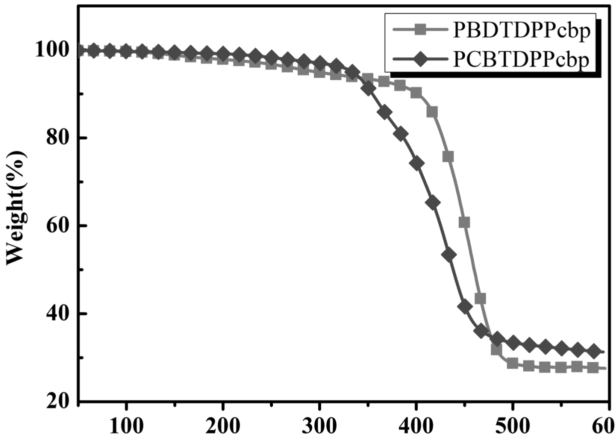

FIGURE 1 TGA curves of polymers with a heating rate of 10 °C/min.

The thermal stability of polymers is an important parameter for optoelectronic device, which can be investigated with TGA. Figure 1 shows that the polymers have good stability and lose 5% weight at the temperature up to 350 °C and 400 °C, respectively. Cyanobiphenyl mesogenic appendages may have well wrapped the conjugated backbones and thus protect them from the perturbation by heat and degradative species.[28] Good thermal stability against oxygen ensures both polymers for device fabrication process and other kinds of applications.

The mesomorphic behavior of polymers has been studied by DSC (see Supporting Information Fig. S4) and POM (Fig. 2). The POM observation of monomer TDPPcbp and copolymers reveals that a bright colorful texture of an enantiotropic mesophase is formed when the sample is cooled and heated. With the aid of XRD measurements, the mesophases have been identified to a nature of two-domain order Smectic A phase. The result is also supported by DSC analysis. For polymer PBDTDPPcbp, DSC reveals two discrete exothermic transitions at 149 and 165 °C on second heating scan curves, which corresponds to the solid–mesophase transition and the mesophase–isotropic transition, respectively. However, for copolymer PCBTDPPcbp, DSC reveals two discrete endotherm transitions at 142 °C and 175 °C. Thus, spontaneous orientation of mesogens has effectively driven the self-assembly of the copolymers, which could provide a favorable pathway for charge transportation.

UV–vis–NIR absorption spectra (Fig. 3) give information regarding the electronic structure of the polymers. Both polymers show well-defined vibronic features in solution at room temperature with λ_{max} at 764 nm for PBDTDPPcbp

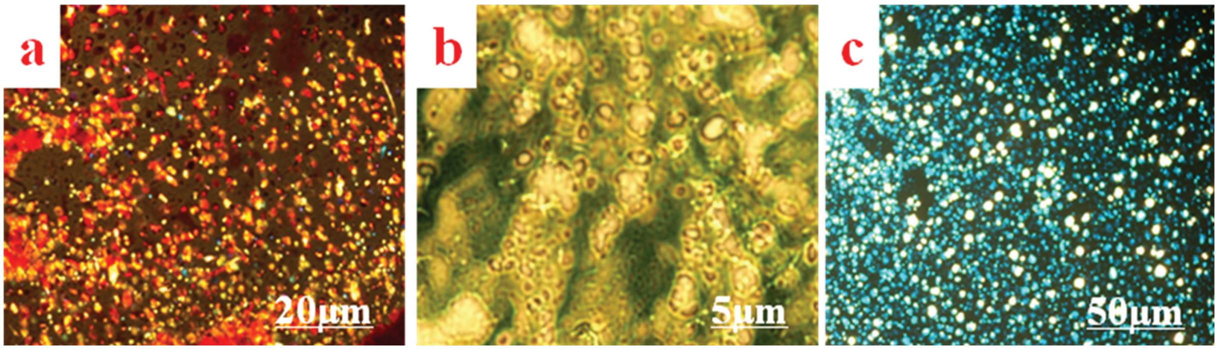

FIGURE 2 The mesomorphic textures observed by POM at LC state. (a) TDPPcbp, (b) PBDTDPPcbp, and (c) PCBTDPPcbp.

and 655 nm for PCBTDPPcbp. The UV–vis absorption peaks of crystalline π-conjugated polymers films are usually bathochromic shift relative to the solution, which is as result of increasing intermolecular interactions between the polymer chain and polymer backbone in the solid state.[31–34] Both polymers show broad absorption spectra with extended absorption edge in the solid state, and bathochromic shift can be observed by 8 nm for PBDTDPPcbp and 28 nm for PCBTDPPcbp, relative to those measured in solution. The peak 300 nm corresponds to the cyanobiphenyl pendants. The films of PBDTDPPcbp and PCBTDPPcbp also exhibit ICT band at 772 nm and 683 nm, respectively. PBDTDPPcbp shows a red-shifted absorption maximum in the film by 90 nm compared to PCBTDPPcbp, maybe due to the higher degree coplanar of PBDTDPPcbp favoring a better stacking in the solid state. This also indicates that the change of donor moiety have an important effect on electron delocalization with the conjugated system. The absorption spectra of the annealed films are shown in Figure 4. Compared to those of films as cast, both PBDTDPPcbp and PCBTDPPcbp annealed films show slightly red-shifted bands and higher absorption intensity as the annealing temperature falls into mesophase region (150 °C), suggesting the mesophase pendant induced the stronger intermolecular interaction and ordered packing arrangement in polymers.

Solid-state packing plays an important role in the electronic properties of conjugated polymers.[35–37] XRD has been used

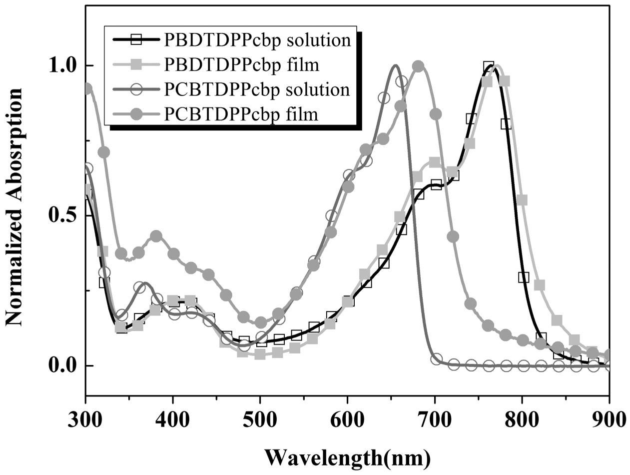

FIGURE 3 UV–vis absorption spectra of copolymers in CF solution and in the solid state.

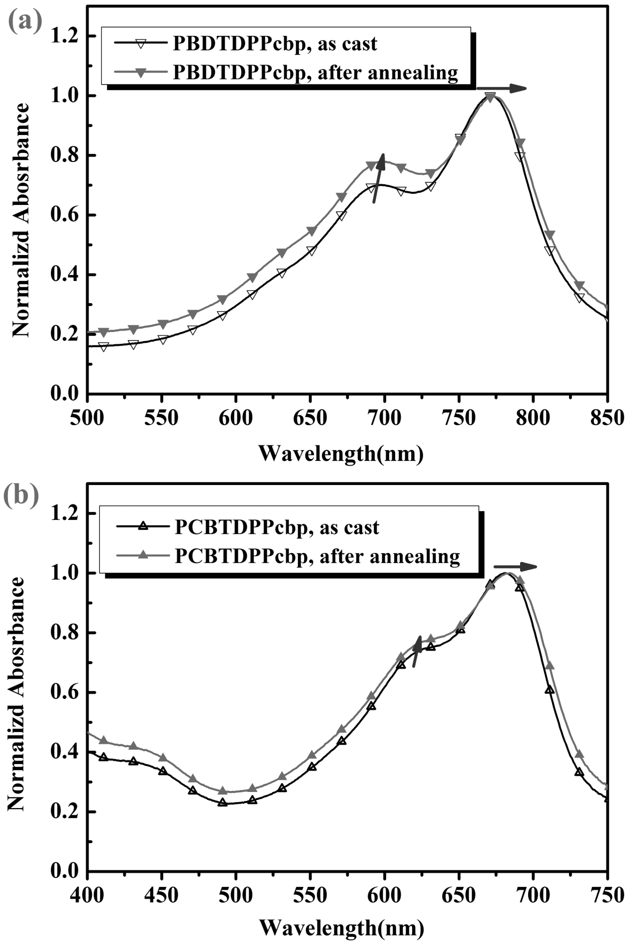

FIGURE 4 UV–vis films absorption spectra of copolymers in solid state at different treatments on a quartz plate. (a) PBDTDPPcbp as cast and after annealing 150 °C and (b) PCBTDPPcbp as cast and after annealing at 150 °C. All the thermal treatments are conducted at such condition except special instructions.

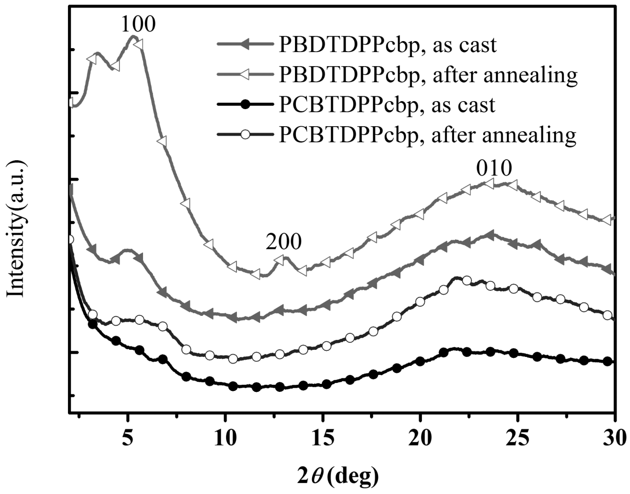

FIGURE 5 XRD patterns of polymer films as cast and after thermal annealing at LC states (150 °C for 0.5 h).

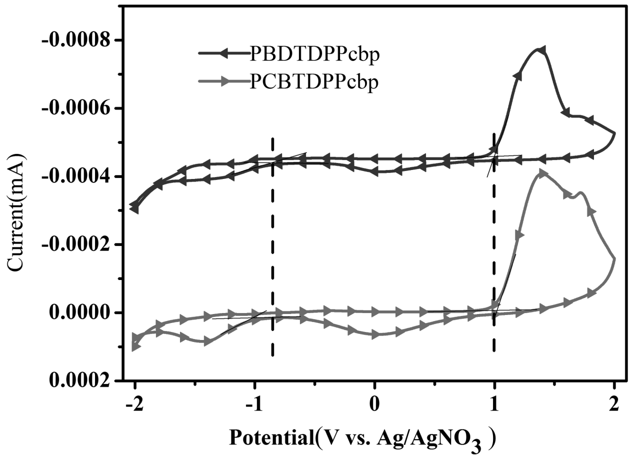

FIGURE 7 CV of polymers films coated on platinum electrode.

to investigate the structural changes of polymer films before and after annealing treatments at LC states (Fig. 5). Compared to the as-cast film, the annealed ones show relatively sharper peaks in the region of 2–30°, especially annealed from the LC state (See supporting Information Fig. S5), which suggests that the formation of more well-ordered crystalline nanostructure can be induced by oriented cyanobiphenyl after LC thermal annealing.[38,39] Distinct primary diffraction features are observed at 2θ of 6.37° for PCBTDPPcbp, which corresponds to the laying distance ($d =$ 1.54 nm), between the sheets of PCBTDPPcbp chains associated with the plane perpendicular to their longitudinal axes. In contrast with PCBTDPPcbp, PBDTDPPcbp exhibit a higher degree of solid state ordering. There are two low-angle Bragg reflections at 2θ of 3.40° and 5.29°, associated to the layer spacing ($d = 2.88$ nm) and molecular length ($d = 1.85$ nm), respectively, and $2\theta = 13°$ ($d = 0.75$ nm) corresponds to biphenyl mesogenic unit length in vertical orientation.

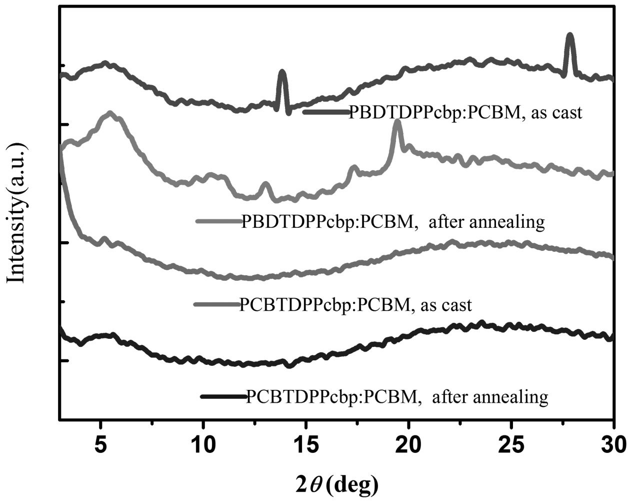

FIGURE 6 XRD spectra of polymers:PCBM (1:2 wt %) films at different treatments: as cast and thermal annealing from LC states (150 °C for 0.5 h).

Thermal treatments also have profound effects on the blend morphology of the active layer of the BHJ.[40,41] To further investigate the microstructure of polymer:PCBM blend films as cast and after thermal annealing, we conducted XRD on the PBDTDPPcbp:PCBM (1:2 wt %) and PCBTDPPcbp: PCBM (1:2 wt %) films at different treatments, respectively. The curves are shown in Figure 6, and the increasing crystalline of blend films suggest that the spontaneous assembly of the LC molecules with PCBM blend films form oriented layer nanostructure after annealed at LC states, especially for the PBDTDPPcbp blending.

Electrochemical CV has been widely used to investigate the redox behavior of the polymer and to estimate its HOMO and LUMO energy levels as well as electrochemical band gap (E_g^{ec}).[42] Figure 7 displays the CV of PBDTDPPcbp and PCBTDPPcbp films on a Pt electrode in a 0.1 mol/L Bu_4NPF_6-CH_3CN solution. The results of the electrochemical measurements are listed in Table 1. It can be seen that there are reversible *n*-doping/dedoping (reduction/reoxidation) processes in the negative and positive potential range for the polymers. The onset oxidation potential (E_{ox}) is 0.99 eV versus $Ag/AgNO_3$ for PBDTDPPcbp and 1.03 eV for PCBTDPPcbp, the HOMO changes very slightly from −5.39 eV for PBDTDPPcbp to −5.43 eV for PCBTDPPcbp. However, PBDTDPPcbp (−3.57 eV) has a low-lying LUMO than PCBTDPPcbp (−3.38 eV). This contributes to PBDTDPPcbp with a lower band gap. Meanwhile, it also indicates that the donor moiety modification has a distinct effect on the energy levels of the polymers. Additionally, polymer PCBTDPPcbp possesses a low-lying HOMO energy level, probably providing an increased open-circuit voltage than that of PBDTDPPcbp.

The photovoltaic properties of the polymers were studied in solar cells with structures of ITO/PEDOT: PSS/ Polymer:[60]PCBM (1:2 wt %)/LiF/Al. Figure 8 shows the

TABLE 1 Electrochemical Properties and Key Polymer Properties of the Copolymers

Polymers	$E_{onset/ox}$ (eV)	$E_{onset/red}$ (eV)	HOMO (eV)	LUMO (eV)	E_g (eV)	M_n/PDI (kg/mol)
PBDTDPPcbp	0.99	−0.83	−5.39	−3.57	1.82	33.0/2.21
PCBTDPPcbp	1.03	−1.02	−5.43	−3.38	2.05	28.1/2.52

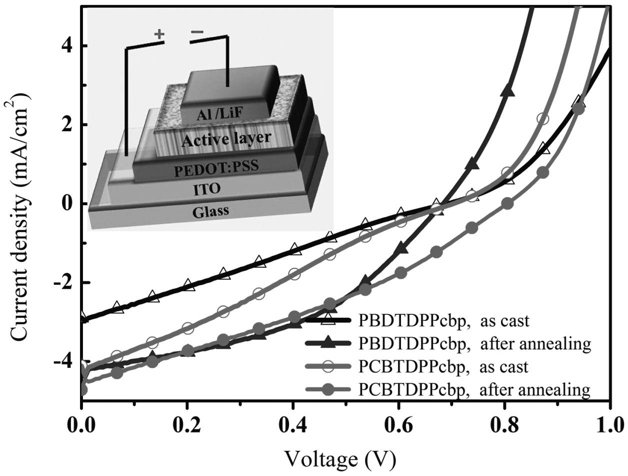

FIGURE 8 *J–V* characteristics of photovoltaic cells based on polymer:PCBM blend films (as cast and thermal annealing from LC states at 150 °C for 10 min) under AM 1.5 G illumination from a calibrated solar simulator with 100 mW/cm^2. Inset is a schematic of device architecture. PBDTDPPcbp:PCBM (1:2 wt %) and PCBTDPPcbp:PCBM(1:2 wt %).

J–V curves for solar cells under AM 1.5 G radiation (100 mW/cm^2). BHJ solar cells were fabricated using PBDTDPPcbp:PCBM and PCBTDPPcbp:PCBM blends as active layer, and the results are outlined in Table 2. We report here preliminary results of thermal-annealed BHJ solar cell. PBDTDPPcbp-based BHJ solar cells demonstrated a short-circuit current (J_{SC}) of 4.11 mA/cm^2, a fill factor (FF) of 0.45, and an open circuit voltage (V_{OC}) of 0.68 V, leading to a PCE of 1.3% after annealing at mesophase. Conversely, compared to PBDTDPPcbp, PCBTDPPcbp has a higher short-circuit current J_{SC} of 4.72 mA/cm^2, but a lower FF of 0.32, a higher open-circuit voltage of 0.80 V, resulting in PCE of 1.2%. Meanwhile, the theoretical V_{OC} of PCBTDPPcbp and PBDTDPPcbp are 0.83 V and 0.79 V, respectively. The V_{OC} of PCBTDPPcbp is also higher than that of PBDTDPPcbp, which is in agreement well with measured value. Nevertheless, the experimental V_{oc} is lower than the theoretical value, probably due to the unfavorable ohmic contact with the electrode and the field-driven photocurrent in BHJ devices.[43] *I–V* curves for PBDTDPPcbp and poly[N-9'-heptadecanyl-2,7-carbazole-alt-3,6-bis(thiophen-5-yl)-2,5-bis[4-(4'-cyano-biphenyloxy) dodecyl]-2,5-dihydropyrrolo[3,4-c]pyrrole-1,4-dione] (PCBTDPPcpb) as cast films show an "s-shaped" kink, resulting from the defects of active layer.[44] After thermal annealing at LC states, the PCE of polymer:PCBM have an increase trend with a higher FF and J_{SC}, which may be due to the optimized morphology. It is firmly believed that by optimizing the interpenetrating network morphology of the DPP-based devices through different polymer/acceptor ratios or annealing treatment, higher FF and PCE value would be obtained.

It is proven that the photovoltaic properties of BHJ relate with the mixing morphology of the polymer and PCBM composite film, which mainly affects the interpenetrated network of the donor and the acceptor.[45] Tapping mode atomic force microscope (AFM) is used to observe the surface morphological structure of the active layer and the phase images are shown in Figure 9. AFM data are consistent with the FF and J_{SC} data of the corresponding devices. Both polymer:PCBM-annealed films show uniform and distinct phase separated structure compared to the as-cast films, which contribute to form channels in the fullerene matrix. The phase-separation appearance is decreasing after annealing while the height images RMS are from 1.69 to 1.12 nm for PCBTDPPcbp before and after thermal annealing, respectively (See Supporting Information Fig. S6). The surface morphology is quite smooth and homogeneous after annealing, which would create excellent phase separation interfaces for charge separation and provide favorable channels for electrons and holes transportate to respective electrodes, consequently reduce the electron-hole recombination ratio.[46] That is why the FF and J_{SC} data of the corresponding devices after annealing have an increased tendency. This observation is

TABLE 2 Device Performances of Polymers:PCBM (w/w 1:2) BHJ Solar Cells Before and After Annealing Using Dichlorobenzene (under A.M. 1.5, 100 mW/cm^2 irradiation)[a]

Device	Thickness (nm)	V_{OC} (V)[b]	J_{SC} (mA/cm^2)[c]	FF[d] (%)	PCE [highest] (%)
PBDTDPPcbp:PCBM (1:2)	150	0.68	2.90	25.7	0.4 ± 0.1 [0.5]
PBDTDPPcbp:PCBM (1:2)-annealed[e]	150	0.68	4.11	44.8	1.2 ± 0.1 [1.3]
PCBTDPPcbp:PCBM (1:2)	150	0.69	4.28	26.0	0.7 ± 0.1 [0.8]
PCBTDPPcbp:PCBM (1:2)-annealed	150	0.80	4.72	31.9	1.1 ± 0.1 [1.2]

[a] All values represent averages from six 0.04 cm^2 devices on a single chip.

[b] V_{OC} is the open-circuit voltage.

[c] J_{SC} is the short-circuit current.

[d] FF is a graphic measure of the *J–V* curve.

[e] The devices were annealed at LC state for 10 min.

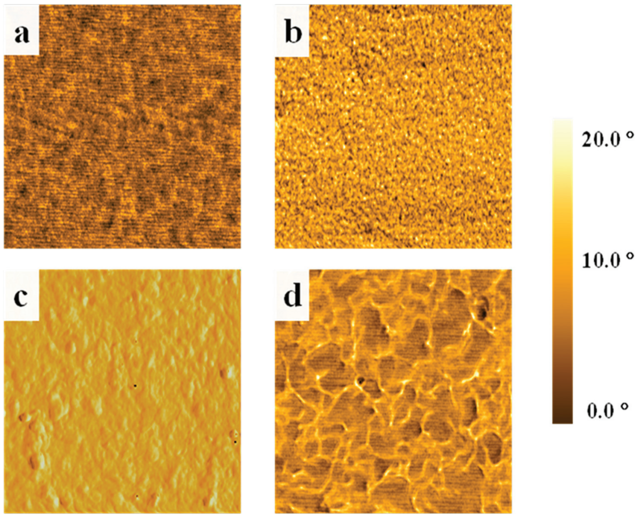

FIGURE 9 Tapping mode AFM phase images of the films based on polymers:PCBM (1:2 wt%) as cast and after annealing from LC states at 150 °C for 10 min (3 μm × 3 μm). (a) PCBTDPPcbp:PCBM, as cast, (b) PCBTDPPcbp:PCBM, after annealing, (c) PBDTDPPcbp:PCBM, as cast, (d) PBDTDPPcbp:PCBM, after annealing.

similar to our previous work that cyano biphenyl mesogenic pendants induced well-ordered active layers morphology after thermal treatment at LC states.[28] Figure 9(d) shows the surface topography of PBDTDPPcbp film after annealing from LC states. The surface comprises of nanofibers with the average width of approximately 30 nm. This nanoscale microphase separation morphology originating from the spontaneous assemblies of LC polymer is highly desirable for BHJ active layer, which also can explain the enhanced performance for PBDTDPPcbp after annealed from LC state.

CONCLUSIONS

Two new type semiconducting conjugated polymers PBDTDPPcbp and PCBTDPPcbp bearing LC side chain were designed and synthesized. It was found that the donor-part variation in the polymers lead to the different electronic properties, as polymer PCBTDPPcbp possesses a low-lying HOMO energy level to provide a higher open-circuit voltage. The LC polymers show red-shifted and enhanced absorption bands after thermal annealing, suggesting that the incorporation of mesogenic pendants could enhance the orientation degree of the polymer. The more ordered lamella structures of the polymers after annealing can also be confirmed from the XRD results. Moreover, thermal-annealed PBDTDPPcbp:PCBM and PCBTDPPcbp:PCBM blend films lead to enhanced PCE of 1.3% and 1.2%, respectively. It is worthy to note that highly desired active layer morphology can be obtained through thermal annealing from the LC state. The performance of the devices is not sufficient to reach the level for solar cells application, but study of the relation between LC and the morphology of the active layer blend has revealed that the LC thermal treatment can enable the bulk form well-connected nanoscale phase separation, consequently enhance the device performance. Thus, incorporation of the mesogens into the conjugated polymers is an effective approach to realize morphology control and LC TDPPcbp is also a kind of promising acceptor segment for the design of D–A type photovoltaic polymers.

ACKNOWLEDGMENTS

This work was supported by the National Natural Science Foundation of China (51073076, 51273088, 51003045, and 51263016).

REFERENCES AND NOTES

1 Liang, Y.; Xu, Z.; Xia, J.; Tsai, S. T.; Wu, Y.; Gang, L.; Ray, C.; Yu, L. *Adv. Mater.* **2010,** *22*, E135–E138.

2 Chu, T. Y.; Lu, J.; Beaupre, S.; Zhang, Y.; Pouliot, J. R.; Wakim, S.; Zhou, J.; Leclerc, M.; Li, Z.; Ding, J.; Tao, Y. *J. Am. Chem. Soc.* **2011,** *133*, 4250–4253.

3 Price, S. C.; Stuart, A. C.; Yang, L.; Zhou, H.; You, W.; *J. Am. Chem. Soc.* **2011,** *133*, 4625–4631.

4 Zhou, H.; Yang, L.; Stuart, A. C.; Price, S. C.; Liu, S.; You, W. *Angew. Chem., Int. Ed.* **2011,** *50*, 2995–2998.

5 Hou, L.; Zhang, S.; Guo, X.; Xu, F.; Li, Y.; Hou, J. *Angew. Chem., Int. Ed.* **2011,** *50*, 9697–9702.

6 He, Z.; Zhong, C.; Huang, X.; Wong, W.; Wu, H.; Chen, L.; Su, S.; Cao, Y.; *Adv. Mater.* **2011,** *23*, 4636–4643.

7 Roncali, J. *Chem. Rev.* **1997,** *97*, 173–205.

8 Chen, H. Y.; Hou, J.; Zhang, S.; Liang, Y.; Yang, G.; Yang, Y.; Yu, L.; Wu, L.; Li, G. *Nat. Photonics* **2009,** *3*, 649–653.

9 Liang, Y.; Feng, D.; Wu, Y.; Tsai, S. T.; Li, G.; Ray, C.; Yu, L. *J. Am. Chem. Soc.* **2009,** *131*, 7792–7799.

10 Blouin, N.; Michaud, A.; Gendron, D.; Wakim, S.; Blair, E.; Plesu, R. N.; Belletête, M.; Durocher, G.; Tao, Y.; Leclerc, M. *J. Am. Chem. Soc.* **2008,** *130*, 732–742.

11 Zhang, Y.; Chien, S. C.; Chen, K. S.; Yip, H. L.; Sun, Y.; Davies, J. A.; Chen, F. C.; Jen, A. K. Y. *Chem. Commun.* **2011,** *47*, 11026–11028.

12 Bronstein, H.; Chen, Z. Y.; Ashraf, R. S.; Zhang, W. M.; Du, J. P.; Durrant, J. R.; Tuladhar, P. S.; Song, K.; Watkins, S. E.; Geerts, Y.; Wienk, M. M.; Janssen, R. A. J.; Anthopoulos, T.; Sirringhaus, H.; Heeney, M.; McCulloch, I. *J. Am. Chem. Soc.* **2011,** *133*, 3272–3275.

13 Woo, C. H.; Beaujuge, P. M.; Holcombe, T. W.; Lee, O. P.; Fréchet, J. M. J. *J. Am. Chem. Soc.* **2010,** *132*, 15547–15549.

14 Bijleveld, J. C.; Zoombelt, A. P.; Mathijssen, S. G. J.; Wienk, M. M.; Turbiez, M.; de Leeuw, D. M.; Janssen, R. A. J. *J. Am. Chem. Soc.* **2009,** *131*, 16616–16617.

15 Bijleveld, J. C.; Gevaerts, V. S.; Di Nuzzo, D.; Turbiez, M.; Mathijssen, S. G. J.; de Leeuw, D. M.; Wienk, M. M.; Janssen, R. A. *J. Adv. Mater.* **2010,** *22*, E242–E246.

16 Li, Y. N.; Sonar, P.; Singh, S. P.; Soh, M. S.; van Meurs, M.; Tan, J. *J. Am. Chem. Soc.* **2011,** *133*, 2198–2204.

17 Sonar, P.; Singh, S. P.; Li, Y.; Soh, M. S.; Dodabalapur, A. *Adv. Mater.* **2010,** *22*, 5409–5413.

18 Nelson, T. L.; Young, T. M.; Liu, J. Y.; Mishra, S. P.; Belot, J. A.; Balliet, C. L.; Javier, A. E.; Kowalewski, T.; McCullough, R. D. *Adv. Mater.* **2010,** *22*, 4617–4621.

19 van Duren, J. K. J.; Dhanabalan, A.; van Hal, P. A.; Janssen, R. A. J. *Synth. Met.* **2001,** *121*, 1587–1588.

20 Dhanabalan, A.; van Duren, J. K. J.; van Hal, P. A.; van Dogen, J. L. J.; Janssen, R. A. J. *Adv. Funct. Mater.* **2001,** *11*, 255–262.

21 Neugebauer, H.; Brabec, C. J.; Sariciftci, N. S.; Kiebooms, R.; Wudl, F.; Luzzati, S. *J. Chem. Phys.* **1999,** *110*, 12108–12115.

22 Percec, V.; Asandei, A. D.; Hill, D. H.; Crawford, D. *Macromolecules* **1999,** *32*, 2597–2604.

23 Percec, V.; Obata, M.; Rudick, J. G.; De, B. B.; Glodde, M.; Bera, T. K.; Magonov, S. N.; Balagurusamy, V. S. K.; Heiney, P. A. *J. Polym. Sci. Part A: Polym. Chem.* **2002,** *40*, 3509–3533.

24 Percec, V.; Rudick, J. G.; Peterca, M.; Wagner, M.; Obata, M.; Mitchell, C. M.; Cho, W. D.; Balagurusamy, V. S. K.; Heiney, P. A. *J. Am. Chem. Soc.* **2005,** *127*, 15257–15264.

25 Rudick, J. G.; Percec, V. *Acc. Chem. Res.* **2008,** *41*, 1641–1652.

26 Percec, V.; Rudick, J. G.; peterca, M.; Heiney, P. A. *J. Am. Chem. Soc.* **2008,** *130*, 7503–7508.

27 Percec, V.; Aqad, E.; Peterca, M; Rudick, J. G.; Lemon, L.; Ronda, J. C.; De, B. B.; Heiney, P. A.; Meijer, E. W. *J. Am. Chem. Soc.* **2006,** *128*, 16365–16372.

28 Yao, K.; Chen, Y. W.; Chen, L.; Li, F.; Li, X. E.; Ren, X. Y.; Wang, H. M.; Liu, T. X. *Macromolecules* **2011,** *44*, 2698–2706.

29 Zou, Y. P.; Gendron, D.; Badrou-Aïch, R.; Najari, A.; Tao, Y.; Leclerc, M. *Macromolecules* **2009,** *42*, 2891–2894.

30 Li, Z.; Zhang, Y. G.; Tsang, S. W.; Du, X. M.; Zhou, J. Y.; Tao, Y.; Ding, J. F. *J. Phys. Chem. C* **2011,** *115*, 18002–18009.

31 Akagi, K. *J. Polym. Sci. Part A: Polym. Chem.* **2009,** *47*, 2463–2485.

32 Percec, V.; Asandei, A. D.; Hill, D. H.; Crawford, D. *Macromolecules* **1999,** *32*, 2597–2604.

33 Kokudo, H.; Sato, T.; Yamamoto, T. *Macromolecules* **2006,** *39*, 3959–3963.

34 Ong, B. S.; Wu, Y.; Liu, P.; Gardner, S. *J. Am. Chem. Soc.* **2004,** *126*, 3378–3379.

35 van Bavel, S.; Veenstra, S.; Loos, J. *Macromol. Rapid Commun.* **2010,** *31*, 1835–1845.

36 Yang, X.; Loos, J. *Macromolecules* **2007,** *40*, 1353–1362.

37 Giridharagopal, R.; Ginger, D. S. *J. Phys. Chem. Lett.* **2010,** *1*, 1160–1169.

38 Yuan, W. Z.; Tang, L.; Zhao, H.; Jin, J. K.; Sun, J. Z.; Qin, A.; Xu, H. P.; Liu, J.; Yang, F.; Zheng, Q.; Chen, E.; Tang, B. Z. *Macromolecules* **2009,** *42*, 52–61.

39 Olsen, B. D.; Gu, X.; Hexemer, A.; Gann, E.; Segalman, R. A. *Macromolecules* **2010,** *43*, 6531–6534.

40 Po, R.; Maggini, M.; Camaioni, N. *J. Phys. Chem. C* **2010,** *114*, 695–706.

41 Ma, W.; Yang, C. Y.; Gong, X.; Lee, K.; Heeger, A. J. *Adv. Funct. Mater.* **2005,** *15*, 1617–1622.

42 Li, Y. F.; Cao, Y.; Gao, J.; Wang, D. L.; Yu, G.; Heeger, A. J. *Synth. Met.* **1999,** *99*, 243–248.

43 Scharber, M. C.; Mühlbacher, D.; Koppe, M.; Denk, P.; Waldauf, C.; Heeger, A. J.; Brabec, C. J. *Adv. Mater.* **2006,** *18*, 789–794.

44 Cheun, H.; Fuentes-Hernandez, C.; Zhou, Y.; Potscavage, W. J.; Sung-Jin Kim, J.; Amir Dindar, J. S.; Kippelen B. *J. Phys. Chem. C* **2010,** *114*, 20713–20718.

45 Chen, L. M.; Hong, Z. R.; Li, G.; Yang, Y. *Adv. Mater.* **2009,** *21*, 1434–1449.

46 Li, F.; Chen, W.; Chen, Y. W. *J. Mater. Chem.* **2012,** *22*, 6259–6266.